Journal of Power Sources 192 (2009) 588–598

Contents lists available at ScienceDirect

Journal of Power Sources

journal homepage: www.elsevier.com/locate/jpowsour

Review

Nanostructures and lithium electrochemical reactivity of lithium titanites and titanium oxides: A review

Zhenguo Yang*, Daiwon Choi, Sebastien Kerisit, Kevin M. Rosso, Donghai Wang, Jason Zhang, Gordon Graff, Jun Liu

Pacific Northwest National Laboratory, Richland, WA 99352, USA

ARTICLE INFO

Article history:
Received 3 January 2009
Received in revised form 13 February 2009
Accepted 13 February 2009
Available online 28 February 2009

Keywords:
Li-ion batteries
Anode
Nanostructured materials
Titanium oxides
Titanite

ABSTRACT

Being inherently safe and chemically compatible with the electrolyte, titanium oxide-based materials, including both Li-titanites and various TiO_2 polymorphs, are considered alternatives to carbonaceous anodes in Li-ion batteries. Given the commercial success of the spinel lithium titanites, TiO_2 polymorphs, in particular in nanostructured forms, have been fabricated and investigated for the applications. Nanostructuring leads to increased reaction areas, shortened Li^+ diffusion and potentially enhanced solubility/capacity. Integration with an electron-conductive second phase into the TiO_2-based nanostructures eases the electron transport, resulting in further improved lithium electrochemical activity and the overall electrochemical performance. This paper reviews structural characteristics and Li-electrochemical reactivity, along with synthetic approaches, of nanostructures and nano-composites based on lithium titanites and TiO_2 polymorphs that include rutile, anatase, bronze and brookite.

Contents

1. Introduction

With great success in the portable electronic sector, Li-ion batteries are considered the most promising energy storage technology for hybrid, plug-in hybrid, and electric vehicle applications. It is also among the technologies increasingly interested in to smooth out intermittency of wind and solar power and improve reliability and efficiency of electrical grids. For the emerging large-scale applications, however, fundamental improvements are needed with regard to power, safety, cycle life, cost, etc. [1–5]. Given that the performance of Li-ion batteries strongly depends on the electrodes properties, significant improvement in the electrochemical properties of electrodes materials are essential to meet the demanding requirements of these applications. One example of this improvement is the rapid development of nanomaterials. The size reduction into the nano-scale (<100 nm) leads to increased electrode/electrolyte contact areas and shortened Li^+ transport distance, permitting batteries to operate at higher power [6–9]. The benefits of nanostructuring are in particular applicable to the materials that exhibit low electronic and/or ionic conductivity, while with appropriate reactivity with electrolyte. The increased reactivity to electrolytes due to the size reduction and increased reaction areas may adversely affects the Li-ion battery performance. Among the materials that greatly benefit from nanostructuring are tita-

* Corresponding author. Tel.: +1 509 375 3756; fax: +1 509 375 2186.
E-mail address: Zgary.yang@pnl.gov (Z. Yang).

0378-7753/$ – see front matter © 2009 Elsevier B.V. All rights reserved.
doi:10.1016/j.jpowsour.2009.02.038

nium oxides-based compositions, including both lithium titanites and various polymorphs of TiO_2. Being abundant, low cost, and environmentally benign, along with some performance advantages, nanostructured titanium oxide-based materials have been widely studied and are considered good alternatives to the carbon-based anode materials in some Li-ion batteries. This paper provides an overview on the titanium oxide-based nanostructures and their lithium electrochemical reactivity as anodes in Li-ion batteries, while exploring routes of materials and synthetic modifications for further improved battery performance.

2. Lithium titanites

Interests in titanium oxide-based materials for anode applications can be traced back to the finding of Li-insertion activities in the lithium titanites. Since early 1990s, Dahn, Thackeray, and Ohzuku et al. [10–12] studied and reported Li-insertion properties of spinel oxides $Li_{1+x}Ti_{2-x}O_4$, $0 \le x \le 1/3$. Both metallic $LiTi_2O_4$ and semiconducting $Li_{4/3}Ti_{5/3}O_4$ ($Li_4Ti_5O_{12}$) exhibit similar Li-insertion electrochemistry with Li-insertion potential being 1.36–1.338 V for $LiTi_2O_4$ and 1.55–1.562 V for $Li_4Ti_5O_{12}$, respectively [10,13]. The relatively high potential vs. Li makes the titanite electrodes intrinsically safer compared to graphite, which has an operating voltage close to Li electroplating potential and thus raises concerns over its safety. $Li_4Ti_5O_{12}$ accommodates Li with a theoretical capacity of 175 mAh g^{-1}, based on the mass of the starting host material, according to the equation

$$[Li]^{8a}[Li_{1/3}, Ti_{5/3}]^{16d}[O_4]^{32e} + e^- + Li^+ \leftrightarrow [Li_2]^{16c}[Li_{1/3}, Ti_{5/3}]^{16d}[O_4]^{32e} \quad (1)$$

where the superscripts stand for the number of equivalent sites with Wyckoff symbols for the space group $Fd\bar{3}m$. Li-insertion/deinsertion in the Li-titanites is accompanied by little or no volume change or structural straining. Consequently, these materials have demonstrated excellent cycle life [12]. Their Li^+ diffusion coefficients of about 10^{-6} cm^2 s^{-1} by neutron radiography [14] or 2×10^{-8} cm^2 s^{-1} by electrochemistry have been reported [15].

The titanites have a spinel structure that consists of a cubic close packed oxygen array in which Li occupies tetrahedral (8a) and octahedral (16c, 16d) sites, while Ti is located with part of Li ions at the 16d octahedral sites of a cubic unit cell ($Fd\bar{3}m$) [10–12,16]. The overall Li-insertion capacity is limited by the number of free octahedral sites. In the titanite spinel, the $[Li_{1/3}Ti_{5/3}]O_4$ framework provides a three-dimensional network of channels for facile Li^+ diffusion [17] and exhibits a minimal volume expansion even after full lithiation. Accordingly, the minimal structural change during lithium insertion/extraction makes it an attractive anode for high rate, long-cycle life battery applications. Peramunage and Abraham [16] reported $Li_4Ti_5O_{12}$/PAN electrolyte//$LiMn_2O_4$ batteries that demonstrated an excellent rechargeability at nearly 100% coulombic efficiency at a 1*C* rate. Importantly the authors introduced first time the concept of passivation-free negative electrodes and used aluminum as current collector for the negative electrode.

Given lithium titanites have no side reactions with electrolytes that are directly related to the irreversible capacity, nanostructuring has been employed to improve their Li-intercalation properties by increasing electrode/electrolyte interfacial contact area and facilitating charge transport. Kim and Cho [18] prepared $Li_4Ti_5O_{12}$ nanowires of 150 nm diameter by firing a mixture of $TiO_2 \cdot 1.25H_2O$ nanowires and Li acetates at 800 °C for 3 h. The synthesized spinel nanowires demonstrated a first discharge capacity of 165 mAh g^{-1} at a 1/10*C* rate and 93% capacity retention at 10*C* rate (see Fig. 1). Kavan and Grätzel [19] reported a thin film-nanocrystalline spinel with a thickness of 2.0–6.0 nm, showing an excellent rate capability compared to the composite spinels. The improved performance with nanostructuring, combined with their inherent structural stability, favorable interface chemistry, and safety, make nanostructured lithium titanites an excellent alternative anode for low cost, long-cycle life, high power Li-ion batteries. The nanostructured titanites have been used as anodes in commercial Li-battery systems demonstrated for large-scale applications.

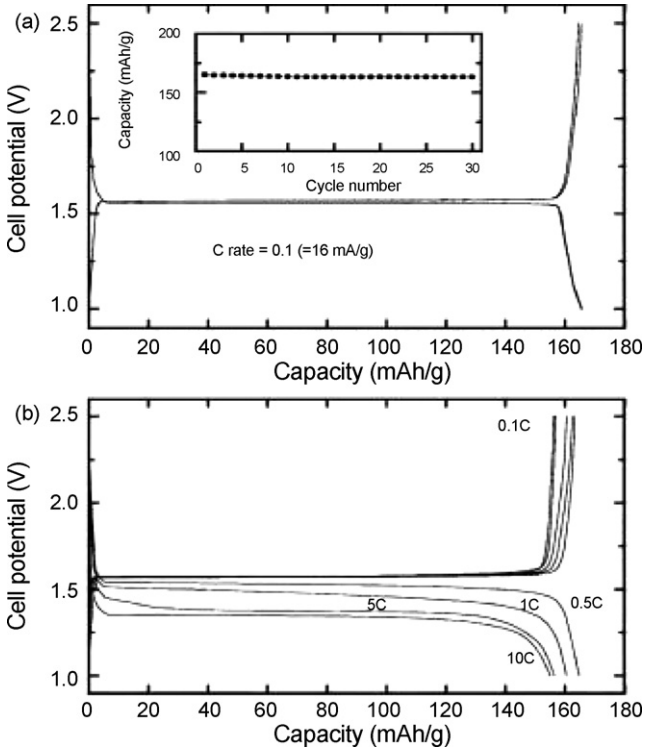

Fig. 1. Voltage profiles of (a) $Li_4Ti_5O_{12}$ nanowires in a coin-type half-cell and discharge capacity as a function of cycle number and (b) rate capability test of the $Li_4Ti_5O_{12}$ nanowires at different *C* rates (0.5, 1, 5 and 10*C*). The charge rate was fixed at 0.1*C* (=16 mA g^{-1}) [18].

3. Titanium oxide (TiO_2) polymorphs

Following the finding of promising Li-insertion properties in the titanite spinels, lately there have been increasing interests in various TiO_2 polymorphs, in particular in their nanostructures for Li-ion battery applications. While $Li_4Ti_5O_{12}$ is an excellent host for reversible Li-insertion/extraction, its specific capacity is limited to 175 mAh g^{-1}. In comparison, TiO_2 offers a capacity up to its theoretical value at 335 or 1.0 Ti per TiO_2. TiO_2 polymorphs reported to date include rutile, anatase, brookite, TiO_2-B (bronze), TiO_2-R (ramsdellite), TiO_2-H (hollandite), TiO_2-II (columbite) and TiO_2-III (baddeleyite). Table 1 lists details of these distinctive polymorph

Table 1
Structural parameters of TiO_2 polymorphs.

Structure	Space group	Density (g cm^{-3})	Unit cell (Å)	Reference
Rutile	$P4_2/mnm$	4.13	$a = 4.59$, $c = 2.96$	[34,35,42]
Anatase	$I4_1/amd$	3.79	$a = 3.79$, $c = 9.51$	[34,35,42]
Brookite	$Pbca$	3.99	$a = 9.17$, $b = 5.46$, $c = 5.14$	[34,36,42]
TiO_2 (B)	$C2/m$	3.64	$a = 12.17$, $b = 3.74$, $c = 6.51$, $\beta = 107.29°$	[34,37,42]
TiO_2-II	$Pbcn$	4.33	$a = 4.52$, $b = 5.5$, $c = 4.94$	[34,38,42]
TiO_2 (H)	$I4/m$	3.46	$a = 10.18$, $c = 2.97$	[34,39,42]
TiO_2-III	$P2_1/c$	C	$a = 4.64$, $b = 4.76$, $c = 4.81$, $\beta = 99.2°$	[40,42]
TiO_2 (R)	$Pbnm$	3.87	$a = 4.9$, $b = 9.46$, $c = 2.96$	[41,42]

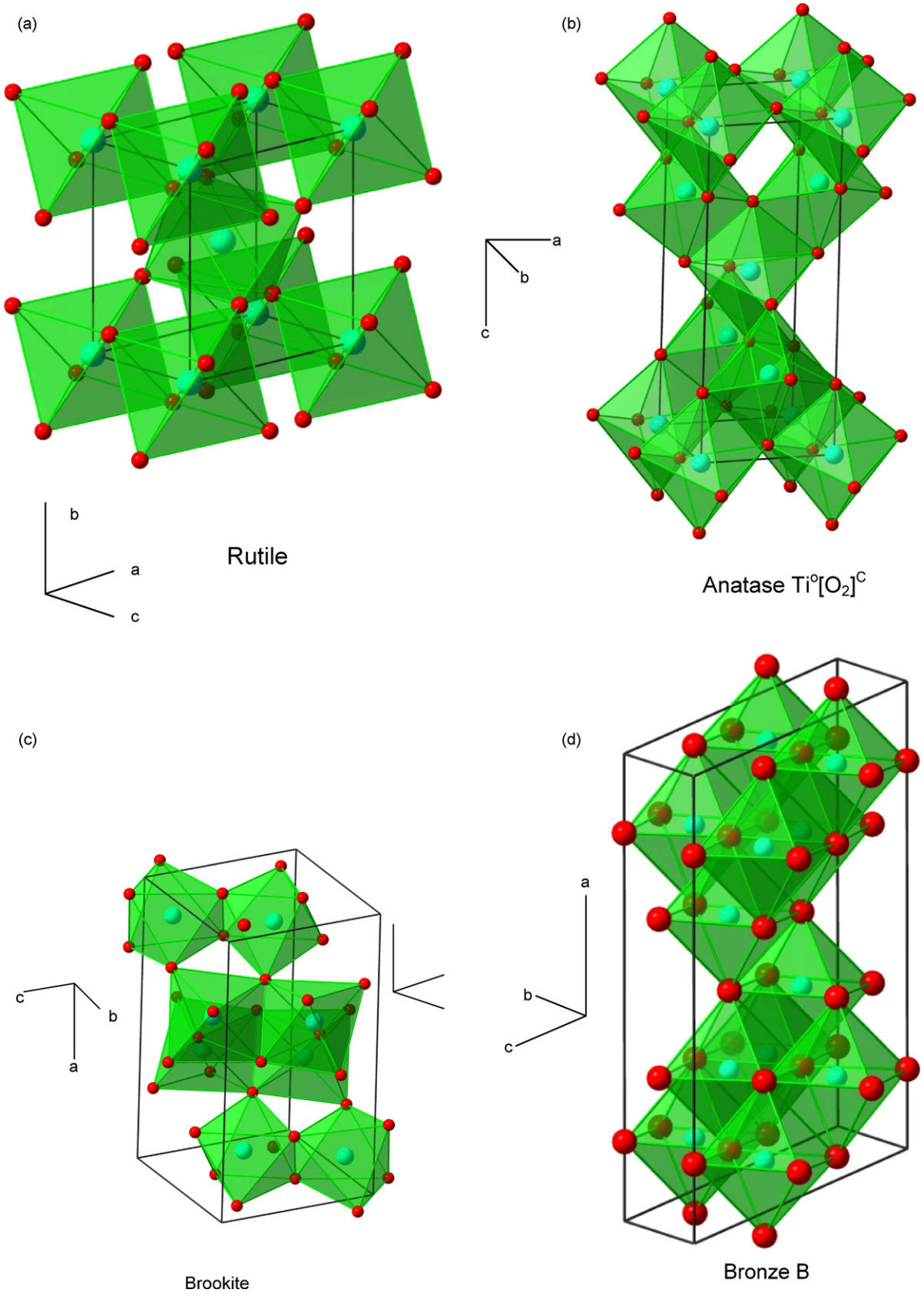

Fig. 2. (a) Rutile, (b) anatase, (c) brookite, and (d) bronze(B) of TiO_2.

structures. Among the TiO_2 polymorphs, rutile, anatase, brookite and TiO_2-B (see Fig. 2) have been reported for Lithium electrochemical reactivity. It is generally considered that at low pressures only rutile has a true field of stability; anatase and brookite form a metastable structure [20,21].

Li-reaction with the TiO_2 polymorphs is conveniently expressed as:

$$xLi^+ + TiO_2 + xe^- \leftrightarrow Li_xTiO_2. \quad (2)$$

This redox reaction implies not only the insertion of xLi^+, but also the creation of charge compensating xTi^{III} cations in the Ti^{IV} sublattice, as observed in X-ray photoelectron spectroscopy experiments [22,23] and supported by theoretical calculations [24–27], with sources of structural strain and relaxation associated with both types of induced defects [28]. The capacity of various TiO_2 polymorphs to undergo this reaction, and relative phase stabilities as a function of Li^+ content, have been examined closely with both experiment and computational molecular modeling. (Experimental studies are reviewed later below.) For modeling studies, both quantum mechanical and empirical potential atomistic modeling have been used to predict relative phase stabilities, but not without occasional contradiction or disagreement with experiment. In one of the earliest molecular modeling studies for this purpose, Mackrodt [26] performed periodic Hartree-Fock structure optimizations for a number of TiO_2 and $LiTiO_2$ polymorphs with great success. Predicted relative stabilities of TiO_2 polymorphs include rutile > anatase > brookite > ramsdellite > spinel, with calculated energy difference between rutile and anatase to be 0.02–0.06 eV, in excellent agreement with density functional theory calculations at the LDA level [29] and the measured ΔH of Navrotsky and Kleppa [30]. More recently, computational studies have focused on the diffusion kinetics of Li^+ in various TiO_2 polymorphs, and have provided insight into the site occupation, local coordination, and energetics that underlie Li mobility [31–33].

The redox reaction defined by Eq. (2) occurs typically at 1.5–1.8 V vs. Li^+/Li redox couple. Similar to the titanites, the relative high potentials make the TiO_2 electrodes inherently safer than the graphite anode and render fewer reactions at the electrode/electrolyte interfaces.

One draw back, however, is the poor conductivity of Li^+ and accompanying electrons in its bulk form, limiting the electrochemical performance of TiO_2 electrode materials. To improve the charge/ion transport properties, TiO_2 polymorphs have been fabricated into varied nanostructures that resulted in improved Li-insertion properties.

3.1. Rutile

As the most thermodynamically stable polymorph of TiO_2, rutile in its bulk crystalline form can only accommodate negligible Li (<0.1 Li per TiO_2 unit) at room temperature [14,43]. Increased Li-reactivity was reported at 120 °C using polymeric rather than liquid electrolyte, with first discharge reversible capacities reaching 0.5 Li [44] and 1 Li [45] per TiO_2 formula unit. It is commonly agreed that Li diffusion in rutile is highly anisotropic, which proceeds through rapid diffusion along *c*-axis channels [46–51]. Experimental and simulation studies showed that the Li^+ diffusion coefficient along *c*-axis is approximately 10^{-6} cm^2 s^{-1} while in the *ab*-plane only about 10^{-15} cm^2 s^{-1} [47,48,52]. Therefore, transport is very slow in the *ab*-planes, restricting Li ions from easily reaching the thermodynamically favorable octahedral sites and limiting Li in the c-channels. Furthermore, repulsive Li–Li interactions in c-channels together with trapped Li-ion pairs in the *ab*-planes may block the c-channels and restrict insertion well below its theoretical limit [48,51].

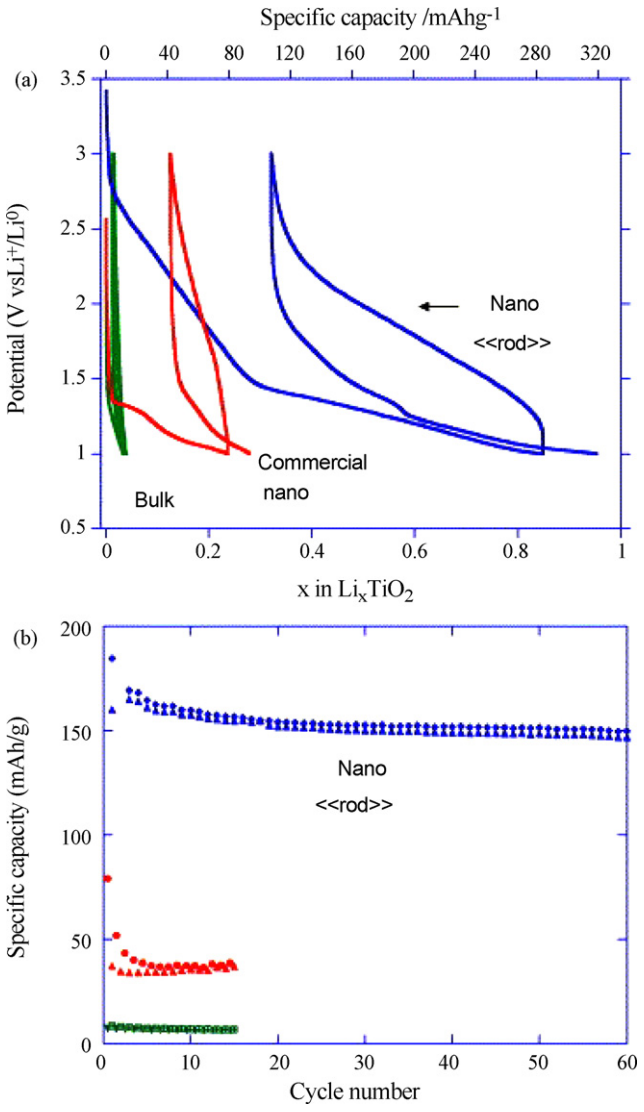

Fig. 3. Galvanostatic cycling curves of rutile TiO_2 samples using a 30 mA g^{-1} current between 3 and 1 V in 1 M $LiPF_6$ EC/DMC electrolyte at 20 °C. The capacity retention is reported for these different samples [54].

Interestingly, however, the Li-reactivity increases with decreasing the particle size. Hu et al. [53] reported up to 0.8 mol Li-insertion into nanostructured rutile TiO_2 (10 nm × 40 nm) at room temperature, while only 0.1–0.25 mol of Li into micrometer-sized rutile. A specific charge of approximately 160 mAh g^{-1} was obtained at a rate of *C*/20 after 50 cycles and that decreased to 150 mAh g^{-1} at *C*/5 and 100 mAh g^{-1} at 10*C*. The authors found that Li-surface storage on the nano-size particles can be energetically more favorable than bulk insertion. Particle size effects were further examined by Baudrin et al. [54], as shown in Fig. 3. The study showed that nano-sized TiO_2 (50 nm) could be inserted up to 0.23 Li per TiO_2 rutile which corresponds to a specific capacity of 77 mAh g^{-1} (at 1/10*C*) during the first reduction down to 1.0 V, out of which 0.11 Li^+ can be extracted during the following oxidation. When the size was decreased to 10 nm, Li-reaction with the nanostructured rutile rod particles (10 nm × 200 nm) was up to 0.85 Li during the first reduction under the same test conditions. The Li-reaction progressed through two solid solution domains, and then through an irreversible phase transformation into electroactive rocksalt type $LiTiO_2$ (ccp) due to the volume expansion in the *ab*-plane. The subsequent oxidation and cycling were carried out on the nanostructured $LiTiO_2$, giving a reversible capacity to 0.5 Li per oxide that

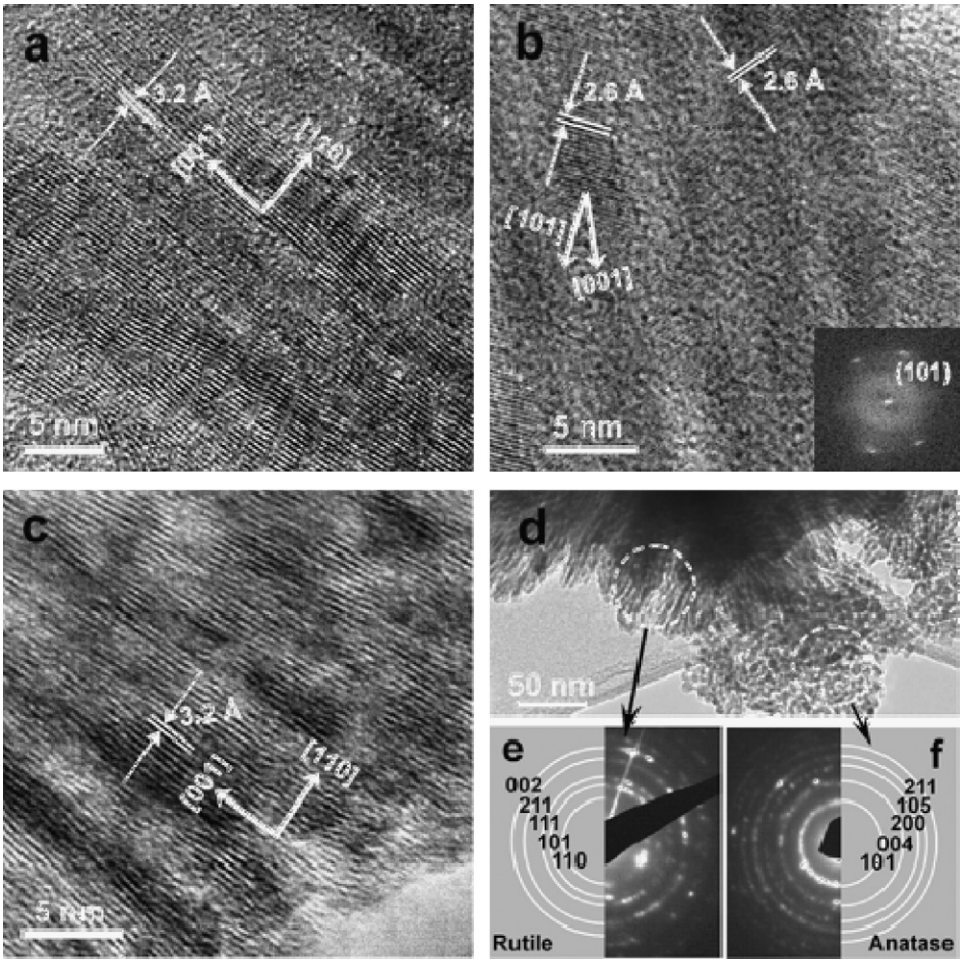

Fig. 4. (a, b) High-resolution TEM images of as-synthesized mesoporous crystalline TiO_2. Inset in (b) shows corresponding SAED pattern. (c) High-resolution TEM image of calcined mesoporous crystalline TiO_2. (d) TEM image of aggregated spherical anatase particles outside of nano-rod-based mesoporous rutile in mesoporous crystalline TiO_2. (e) SAED pattern from the oriented rodlike nanocrystal area circled in (d). The diffraction ring pattern is consistent with that of rutile crystal structure. (f) SAED pattern from spherical nano-particle area circled in (d). The diffraction ring pattern is consistent with that of the anatase crystal structure [58].

is comparable to that of bulk anatase form of TiO_2, which is generally considered to be a more electrochemically active Li-insertion host (to be discussed later). The nano-rutile exhibited smooth and continuous sloping voltage composition curves that resemble the Li-insertion/extraction into layered V_2O_5 [55]. Overall, it appeared that the main kinetic limitations were linked to mechanical strains that were reduced as the particle size decreased, thereby enabling more efficient Li-insertion. This size effect was expected to be more significant for nano-rods aligned along *c*-axis due to the main expansion occurring along the smaller dimension in *ab*-planes. Similarly, Anji Reddy et al. [56] confirmed the Li-insertion up to 1 Li per formula unit at room temperature in nanocrystalline rutile TiO_2 that was synthesized via sol–gel approach. Jiang et al. [57] reported recently that Li-insertion can be up to 1.0 Li per TiO_2 rutile nano-electrodes at the first discharge cycled at 0.05 A g^{-1} (or about 1/6*C*), and 0.6–0.7 Li can be reversibly cycled. After 100 cycles, the discharge capacity of the ultra-fine nano-rutile electrodes was still of 132 and 118 mAh g^{-1} when cycled at 5 and 10 A g^{-1} (or about 16 and 32*C*), respectively.

In addition to the aforementioned nanostructures of the rutile phase, Liu and co-workers [58] recently studied Li-insertion activities in mesoporous rutile TiO_2 (plus a residual amount of anatase) that was synthesized via a new low-temperature solution growth of TiO_2 nanocrystals within an anionic surfactant matrix. The highly crystalline and high surface area (245–300 m^2 g^{-1}) mesoporous TiO_2, as illustrated in Fig. 4, are composed of aligned rutile nano-rod building blocks grown along the [0 0 1] direction. Fig. 5 shows the Li-insertion properties of the new mesoporous crystalline rutile. It could accommodate more than 0.7 Li ($Li_{0.7}TiO_2$, 235 mAh g^{-1}) during the first discharge at a *C*/5 rate between 1 and 3 V vs. Li^+/Li, with a reversible capacity of 0.55 Li ($Li_{0.55}TiO_2$, 185 mAh g^{-1}). The mesoporous crystalline rutile shows excellent capacity retention with less than 10% capacity loss after more than 100 cycles. Their study indicated that the rutile nano-rods were irreversibly transformed into cubic rocksalt $LiTiO_2$ nano-rods during the first discharge. But thereafter the mesostructure of $LiTiO_2$ remained stable during subsequent discharge/charge cycling.

3.2. Anatase

In comparison with the rutile structure, the uptake of Li^+ appears more facile in the anatase lattice. It has a tetragonal body-centered space group $I4_1/amd$, and is comprised of TiO_6 octahedra sharing two adjacent edges with two other octahedra so that planar double chains are formed [59]. Diffusion of Li ions in an anatase framework occurs along a reaction path connecting the octahedral interstitial sites [60,33,31]. With Li-insertion the symmetry of the anatase unit cell decreases and, when $x = 0.5$ ($Li_{0.5}TiO_2$), its original $I4_1/amd$ symmetry transforms into the orthorhombic $Pmn2_1$ space group due to loss of symmetry in the *y* direction [61]. The change in symmetry is accompanied by a decrease of the unit cell along the *c*-axis and an increase along the *b*-axis, resulting in a net increase

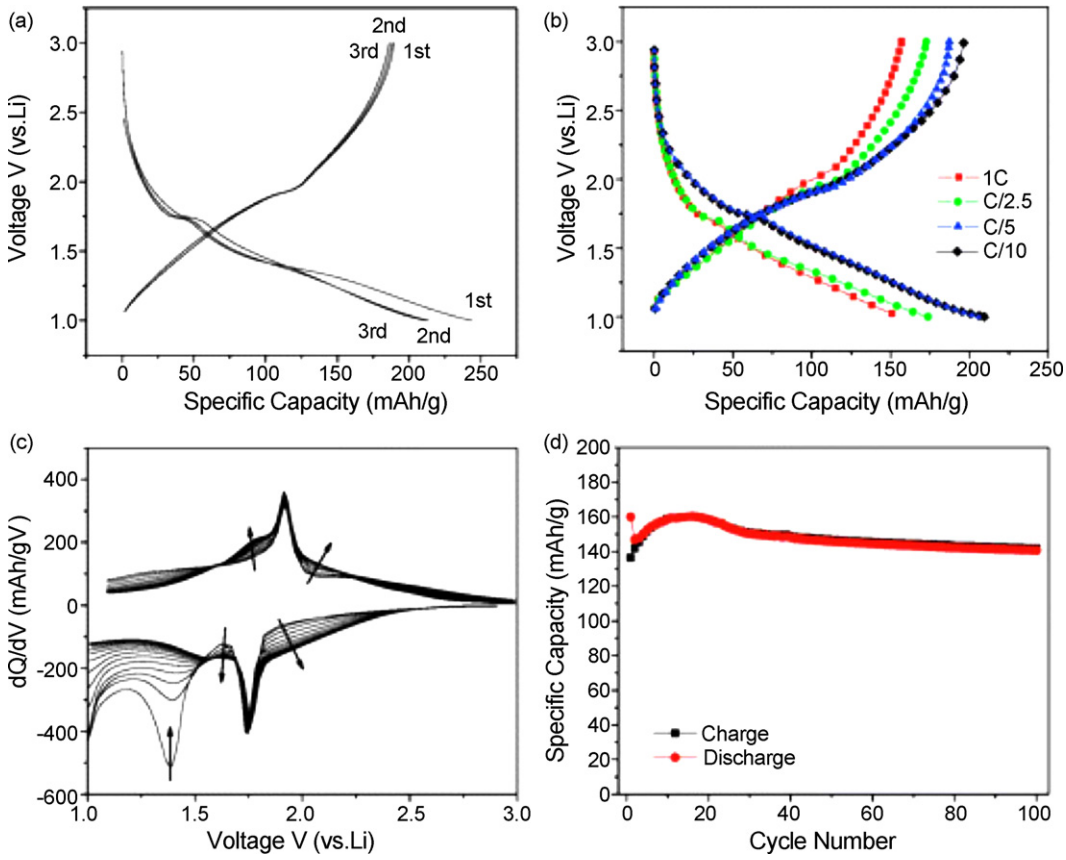

Fig. 5. (a) First three potential-capacity profiles of mesoporous crystalline TiO_2 at a rate of *C*/5 between voltage limits of 1 and 3 V vs. Li^+/Li. (b) Fifth cycle discharge–charge capacity profile of the mesoporous crystalline TiO_2 at the various rate (1*C*–*C*/10) between voltage limits of 1 and 3 V. (c) d*Q*/d*V* vs. potential plot of lithiated/delithiated mesoporous crystalline TiO_2. (d) Cycling behavior of mesoporous crystalline TiO_2 up to 100 cycles at a 1*C* rate [58].

of ~4% of the unit cell volume and a rapid capacity fade [62]. As thus, for bulk anatase, $x = 0.5$ is most consistently reported as the maximum electrochemical insertion of Li [63–66]. Further study by Wagemaker et al. [67–70] found that, during Li-insertion, the anatase undergone spontaneous phase separation into $Li_{0.01}TiO_2$ and $Li_{0.6}TiO_2$ domains on a scale of several tens of nanometers. As shown in Fig. 6, bulk anatase demonstrates flat voltage curves, indicating a classical bi-phase electrochemical reaction process of the Li-insertion/extraction. Similar to the rutile structure, decreas-

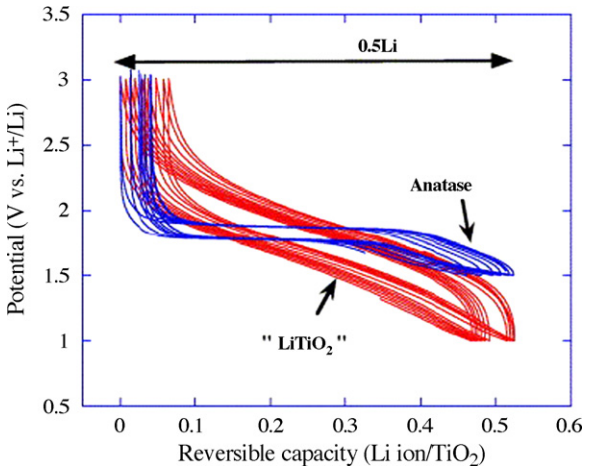

Fig. 6. Comparison between the electrochemical behavior of rutile (nano-rod) and anatase type TiO_2 after the first reduction in a galvanostatic mode with 30 mA g^{-1} between 3 and 1 V in 1 M $LiPF_6$. EC/DMC electrolyte at 20 °C [63].

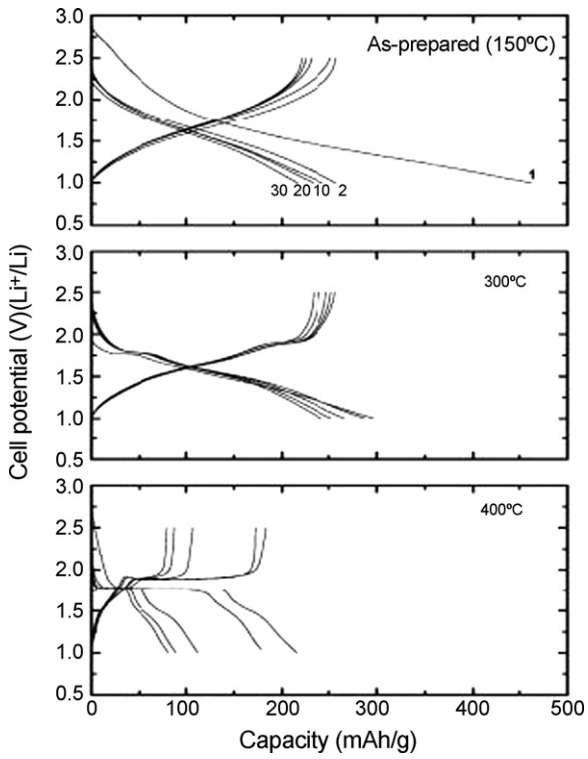

Fig. 7. Nano-anatase TiO_2 voltage profiles of the as-prepared (150 °C), annealed nanotubes (300 °C), and nano-rods (400 °C) between 2.5 and 1 V at a rate of 0.1*C* (=25 mA g^{-1}) after 1st, 2nd, 10th, 20th, and 30th cycles using coin-type half-cells (electrode density was 2 g cm^{-3}) [76].

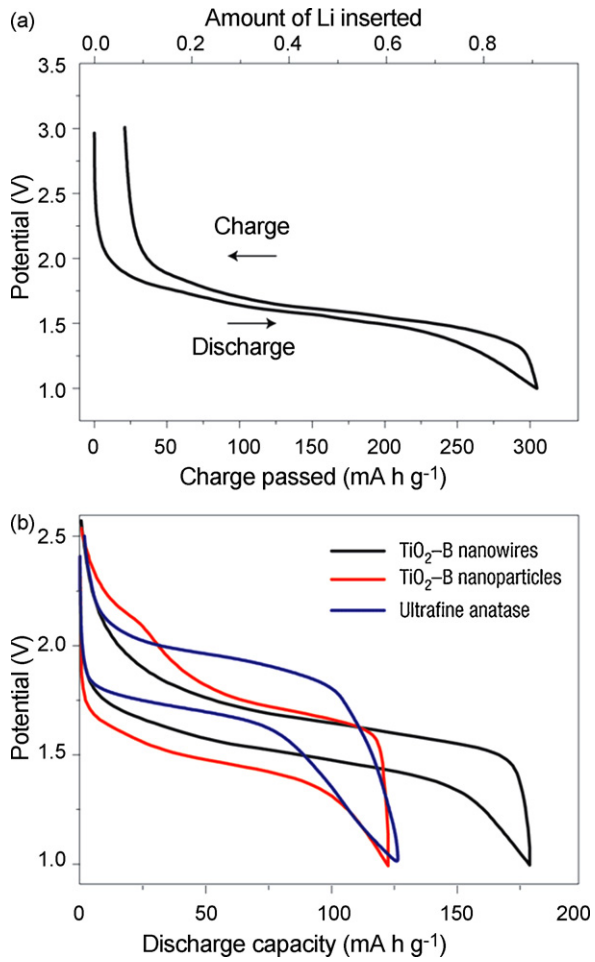

Fig. 8. (a) Charge–discharge curves for Li_xTiO_2-B nanowires (rate of 10 mA g^{-1}); (b) comparison of cycling behavior for TiO_2-B nanowires, TiO_2-B nano-particles and nano-particulate anatase, all at 200 mA g^{-1} [79,80].

ing the particle size into the nano-regime (<100 nm) alternates the electrochemical reactions and reactivity to Li. The Li-interaction with the nanostructures appeared deviating from the two phase equilibrium phenomenon in the bulk materials, instead of behaving more like solid solution [71]. The size reduction, along with unique morphologies, also led to increased capacity over 0.5 Li per unit formula due to the surface-confined charge storage and different Li-reaction mechanisms from that in the bulk materials [72,73]. Gao et al. [74] reported first discharge and charge capacities of 340 and 200 mAh g^{-1}, respectively, for the anatase nanotubes that were synthesized with 10–15 nm outer diameters and 200–400 nm lengths by annealing the hydrothermally prepared protonated nanotubes at 500 °C in an argon atmosphere. Li et al. [63] prepared the anatase TiO_2 nanotubes with outer diameters of 9 nm and several hundred nanometer lengths by annealing at 350 °C using hydrothermal-treated protonated titanate nanotubes. The anatase nanotubes exhibited first discharge and charge capacities 314 and 248 mAh g^{-1}, respectively, but with active material loading only of 3–4 mg cm^{-2}. Zhang and co-workers [75] prepared the anatase nanotubes with diameters of about 10 nm and lengths of 200–400 nm via a hydrothermal approach. The one-dimensional TiO_2 polymorph exhibited a potential plateau at 1.73 and 1.88 V in the process of Li-insertion and extraction, and the initial Li-insertion/extraction capacity is 290 and 238 mAh g^{-1} at 36 mA g^{-1}, respectively.

Kim and Cho [76] reported both anatase TiO_2 nanotubes and nano-rods that were prepared by annealing mixed $H_2Ti_2O_5{\cdot}H_2O$ and anatase TiO_2 nanotubes at 300 and 400 °C, respectively. These two nanostructures exhibited a first discharge capacities of 296 mAh g^{-1} ($Li_{0.88}TiO_2$) and 215 mAh g^{-1} ($Li_{0.64}TiO_2$), respectively, as shown in Fig. 7, in a galvanostatic mode with 25 mA g^{-1} (or about 1/10*C*) between 2.5 and 1 V in 1 M $LiPF_6$ EC/DMC PC electrolyte. Irreversible capacity ratios were reported as 14 and 15% for anatase nanotubes and nano-rods, respectively. Capacity retention of the nanotubes was 81%, compared with only 40% for the nano-rods after 30 cycles. It was found that the high rate performance of nano-rods strongly depended on the electrode density. Nano-rods with 0.5 g cm^{-3} (=12 mg cm^{-2}) showed 200 and 160 mAh g^{-1} at 0.5 and 10*C* rates, respectively. In contrast, nanotubes showed no capacity decrease at 0.5*C* or 10*C* under an electrode density of either 1.0 or 0.5 g cm^{-3}. Under 2 g cm^{-3} (=31 mg cm^{-2}), nanotubes showed 245 and 185 mAh g^{-1} at 0.5 and 2*C* rates, respectively. Recently, Bao et al. [77] reported nano-porous anatase nano-rods that were synthesized by using a binary eutectic mixture system. This novel material exhibited a high-specific surface area with 5 nm pore-size distribution, uniform and regular rod-shaped structures. The nano-porous structure demonstrated a good cyclability and a high rate capability.

3.3. Bronze or TiO_2-B

TiO_2-B was first synthesized by Marchand et al. [37] in 1980 by ion-exchange of K^+ for H^+ in $K_2Ti_4O_9$ to form a hydrated hydro-

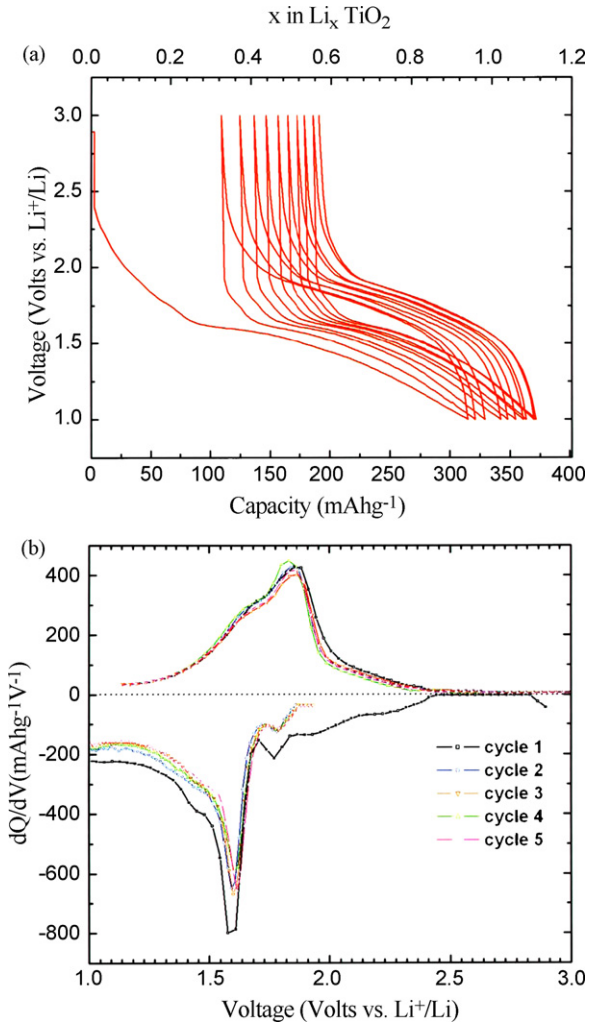

Fig. 9. (a) Voltage-capacity profiles of brookite TiO_2 for the first 10 cycles carried out in the voltage range 1.0–3.0 V at *C*/10 rate; (b) the corresponding differential capacity plot for the first 5 cycles [86].

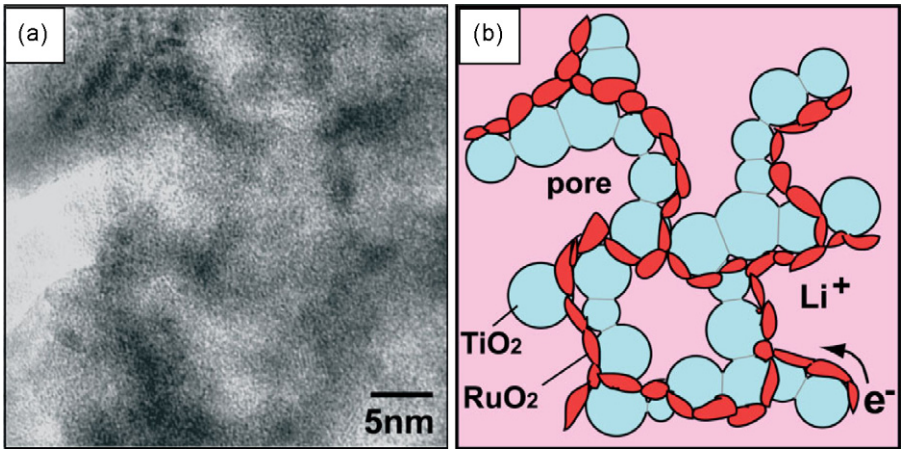

Fig. 10. Elemental mapping of mesoporous TiO_2:RuO_2 nano-composite. (a) Annular dark-field TEM image of mesoporous TiO_2:RuO_2 nano-composite and corresponding Ti and Ru EDX maps; (b) HRTEM image taken from the outer edges of a TiO_2:RuO_2 sphere; (c) corresponding schematic illustration of the self-wired path of deposited RuO_2 nano-particles [87].

gen titanate, which transformed to TiO_2-B during heating at 500 °C. Like rutile and anatase, TiO_2-B is composed of corrugated sheets of edge- and corner-sharing TiO_6 octahedra [78]. But in the case of TiO_2-B, the octahedra are arranged to form perovskite-like pathways along which inserted Li^+ may undergo facile transport. The structure of TiO_2 is more open than other polymorphs, with a density of 3.73 g cm^{-3} compared with 4.25 and 3.89 g cm^{-3} for rutile and anatase, respectively. The open structure may also ease Li^+ transport.

Armstrong, et al. [79–81] prepared TiO_2-B nanowires via hydrothermal reaction between sodium hydroxide, NaOH, and TiO_2 anatase. Subsequent electrochemical evaluation gave a capacity of 305 mAh g^{-1}, or $Li_{0.91}TiO_2$-B, compared with 240 mAh g^{-1} of bulk TiO_2-B. Incremental capacity plots (dQ/dE vs. E) indicated no significant structural change occurring during the Li-insertion/extraction. While the capacity of the TiO_2-B nanowires was comparable to that of nano-particulate TiO_2-B, the nanowires demonstrated superior capacity retention. After 50 cycles, the capacity of the TiO_2-B

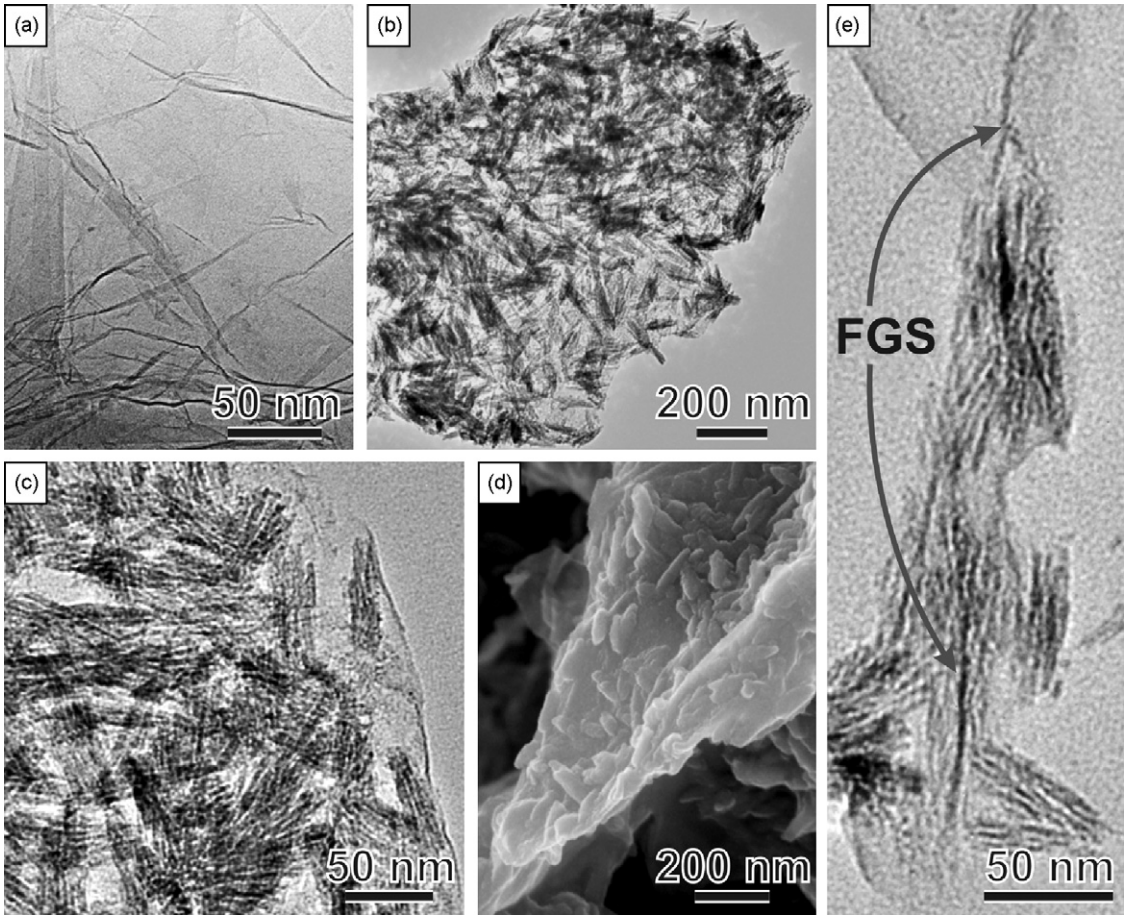

Fig. 11. (a) TEM image of functionalized graphene sheets (FGSs). (b), (c), and (d) Low- and high-magnification TEM and SEM images of the self-assembled rutile TiO_2-FGS hybrids, respectively; (e) A cross-section TEM image of rutile TiO_2-FGS hybrid showing nanostructured rutile TiO_2 lying on the FGS.

nanowires was about twice that of nano-particulate TiO_2-B. It was also reported that the TiO_2-B nanowires performed much better than nano-particle anatase with an average particle size comparable to the diameter of the TiO_2-B nanowires (see Fig. 8). But like the other polymorphs, nanostructured or bulk, there was still an irreversible capacity loss on the first cycle, which was tentatively attributed to the poor conductivity of TiO_2. Lately there have been further insights into Li-reaction with nanostructured TiO_2 (B). Graetzel and co-workers [73] reported and discussed the pseudocapacitive lithium storage in TiO_2 (B). The Li-insertion electrochemistry of TiO_2 (B) appears different from that of anatase. Whereas the kinetics of lithium storage is controlled by solid–solid state diffusion of Li^+, the TiO_2(B) host accommodates lithium by a pseudocapacitive faradic process, which is not controlled by diffusion at comparable conditions.

To further evaluate the electrochemical performance of TiO_2-B nanowires, Armstrong et al. [82] constructed rechargeable lithium-ion batteries with the nanowires as an anode, a gel electrolyte, and either a $LiFePO_4$ or $LiNi_{0.5}Mn_{1.5}O_4$ cathode. Average cell voltages of approximately 2 and 3 V were obtained, respectively. Cycling stability was very good as was rate capability, with 80% of the low-rate capacity being retained at 5*C*. The cells with the TiO_2-B anode demonstrated superior capacity compared to similar batteries constructed using $Li_4Ti_5O_{12}$ (225 mAh g^{-1} compared to 150 mAh g^{-1} at *C*/5) [83].

3.4. Brookite

In addition to rutile, anatase, and bronze structures, brookite was recently investigated for its Li-electrochemical reactivity. Anji Reddy et al. [84,85] reported synthesis of brookite by thermolysis of $TiCl_4$ at 100 °C. The obtained rutile and brookite mixture was separated by peptization in 3 M nitric acid followed by centrifugation. The nano-sized (10 nm) brookite was tested as a Li-ion anode, which delivered reversible capacity of 170 mAh g^{-1} for more than 40 cycles. The specific capacity of brookite varied with the size of the particles, where 20 and 33 nm sized brookite delivered 60 and 35 mAh g^{-1} after 50 cycles, respectively. Also, Lee et al. [86] synthesized brookite by urea precipitation and investigated 10–20 nm sized brookite with multi-walled carbon nanotubes, which delivered 160 mAh g^{-1} over 50 cycles. Li-insertion/extraction was observed at 1.7 and 2.02 V, respectively, compared to 1.64 and 2.1 V for anatase (Fig. 9).

4. Hierarchical, composite nanostructures of TiO_2 polymorphs

As reviewed and discussed previously, nanostructuring TiO_2 polymorphs leads to improved Li-intercalation properties due in part to shortened Li^+-diffusion distances. However, this kind of structural refinement may not concomitantly lead to shortened electron-transport distances if the electron-conductive additive used for the current collector is not sufficiently mixed or similarly structured at nano-scale. Indeed nanostructuring may make it more difficult to mix uniformly a conductive second phase, such as the carbon black at the nano-scale. As a result, the electron transport part may remain sluggish due to the poor conductivity of TiO_2 and thus limit the overall Li-electrochemical activity of the material. For instance, for the nano-particulates, wires and tubes of TiO_2 polymorphs, there is still a substantial irreversible capacity loss during the first cycles likely due to the poor electronic conductivity. Developing nanostructured composite structures that integrate the electron-conductive additive phase appears to be a promising approach due to both shortened Li-transport distances and facile electron transport.

Guo et al. [87] reported superior electrochemical performance of nanostructured mesoporous TiO_2 (anatase) through efficient hierarchical mixed conducting networks. The hierarchically constructed nano-anatase electrode, as shown in Fig. 10, was fabricated with RuO_2, a material with good electrical conductivity, providing highly conducting paths for electrons in a three-dimensional network. This nano-sized network resulted in negligible diffusion times, enhanced local conductivities, possibly faster phase transformation reactions, and hence appeared to be the key to good power performance for the material. While the use of expensive precious metal or its oxide is questionable for commercial applications, integration of conducting additive materials at the nano-scale appears feasible for significant performance improvement. A specific charge capacity of around 214 mAh g^{-1} was obtained at a rate of *C*/5 after 20 cycles, which was lowered to 190, 147, and 125 mAh g^{-1} at 1, 5, and 10*C*, respectively. At the very high rate of 30*C* (discharge/charge of all the TiO_2 within 2 min), the specific charge capacity is still 91 mAh g^{-1}, which is about two times larger than that of 5 nm anatase (48 mAh g^{-1}) and nine times larger than that of mesoporous anatase spheres without interior electronic wiring (10 mAh g^{-1}). The reversibility is demonstrated by the fact that the capacity of 210 mAh g^{-1} is regained if the rate is lowered to *C*/5.

Recently, Liu and co-workers [88] developed self-assembled rutile TiO_2/graphene hybrid nanostructures via anionic surfactant mediated growth. As shown in Fig. 11, the highly electron-conductive graphene, a two-dimensional graphite, is integrated into the nanostructured rutile and acts as the current collector to minimize electrical resistance and power loss of the electrode. As a

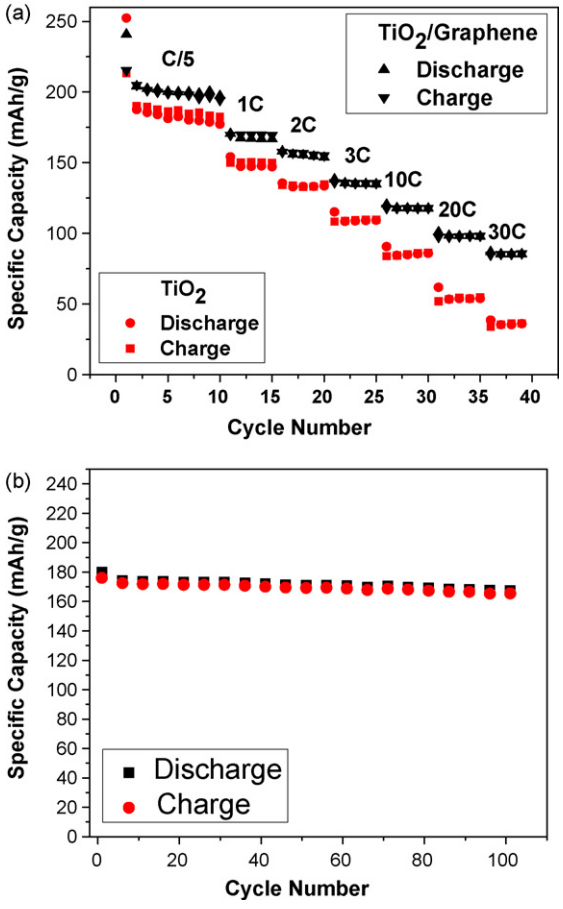

Fig. 12. (a) Specific capacity of nanostructured TiO_2 and nanostructured TiO_2-FGS (functionalized graphene sheet) hybrids (1 wt.% FGS) at different charge/discharge rates, and (b) cycling performance of TiO_2-FGS (1 wt.% FGS) up to 100 cycles at 1*C* charge/discharge rates after testing at various rates [88].

result, this nanostructured material demonstrated enhanced Li-ion insertion/extraction kinetics, especially at high charge/discharge rate, and an excellent cyclability, as shown in Fig. 12. Indeed, the power performance of this nanostructured rutile/graphene composite is indeed comparable or even better to that of the hierarchically constructed composite TiO_2/RuO_2 electrode discussed above. With the incorporation of the functionalized graphene sheets (FGS), specific capacity of the rutile TiO_2 in the hybrids (0.5 wt.% FGS) increased at all charge/discharge rates compared with the control rutile TiO_2. The relative increase in specific capacity is especially larger at higher rates. For instance, at a rate of 30*C*, the specific capacity of the rutile TiO_2-FGS hybrid material is 87 mAh g^{-1} which is more than double the high rate capacity (35 mAh g^{-1}) of the control rutile TiO_2. The rutile TiO_2-FGS hybrids also show good capacity retention of the Li-ion insertion/extraction over 100 cycles at 1*C* rate. Similarly, the anatase TiO_2-FGS hybrid was also synthesized. Like the rutile TiO_2-FGS, specific capacity of the anatase TiO_2-FGS hybrid was enhanced at all charge–discharge rates. The specific capacity of the anatase TiO_2-FGS at rate of 30*C* is as high as 96 mAh g^{-1} compared with 25 mAh g^{-1} of control anatase TiO_2.

In addition, Zhou et al. [89] introduced a new concept in the design of an electrode material having a self-ordered, crystalline-glass, mesoporous nano-composite (CGMN) structure, as shown in Fig. 13. The 5 nm frameworks of the CGMN were assembled in a compact arrangement from electrode-active nanocrystals with a small quantity of glass phase. The 4 nm uniform mesochannels of the CGMN were filled with electrolyte solution to provide

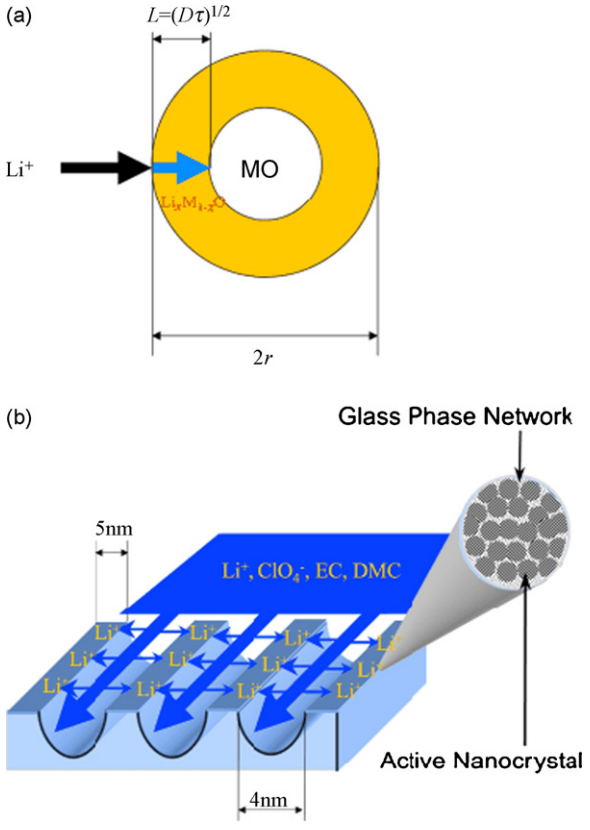

Fig. 13. (a) A schematic representation of the effective diffusion length in electrode-active materials. The area marked in yellow shows the volume reacting with Li^+ ions in the charge/discharge period τ in a diffusion-controlled process. (b) A schematic representation of the reduced diffusion length in a rechargeable battery containing a self-ordered, crystalline-glass, mesoporous nano-composite [89]. (For interpretation of the references to color in this figure legend, the reader is referred to the web version of the article.)

electrolyte and lithium-ion transport pathways throughout the material. In addition, the high surface area of the CGMN reduces the effective specific current density. The three-dimensional glass network in the framework of the CGMN was able to incorporate a high content of electronic conductive oxides above the percolation-threshold value to form an electronic path, and to add lithium ions as a network modifier during the first insertion process to form an ionic path. As a result, the nano-composites demonstrated a significant improvement in specific energy capacities at high current densities.

5. Concluding remarks

Following the commercial success in lithium titanites, particularly in their nanostructures, extensive researches have been carrying out on titanium oxide polymorphs and their composites. Lithium insertion is fairly well understood in the case of anatase and bronze polymorphs. The Li-insertion electrochemistry of TiO_2 (B) appears different from that of anatase. Whereas the kinetics of lithium storage is controlled by solid–solid state diffusion of Li^+, the TiO_2(B) host accommodates lithium by a pseudocapacitive faradic process, which is not controlled by diffusion at comparable conditions. However, lithium insertion into other polymorphs such as rutile and brookite was not well known until very recently, when a high Li-electrochemical activity was reported in nanometer-sized rutile and brookite at room temperature. Generally, nanostructuring led to improved Li-reaction activities due to shortened Li^+-diffusion distances and increased electrode/electrolyte interfacial contact areas, as well as potentially enhanced solubility and capacity. With a much higher diffusivity along the *c*-axis than in the *ab*-plane, rutile nano-rods grown along [0 0 1] direction demonstrated a substantially improved Li-insertion activity. Therefore, Li-insertion activity for TiO_2 polymorphs is not only dependent on the crystal size, but likely also on particle morphology and crystallographic orientation.

Further improvement in the Li-insertion properties was obtained when electron transport was also improved. For TiO_2 polymorphs, this is particularly important given their poor electrical conductivity. Introducing composite nanostructures that integrated an electron-conductive phase at the nano-scale showed remarkable performance enhancement, presumably because of both short Li^+ diffusion distances and improved electron transport. The steadily improving performance of TiO_2 attained through nanostructuring, combined with its inherently favorable interfacial chemistry and safety make nanostructured lithium titanites a promising replacement for graphite in anodes of Li-ion batteries. To gain commercial success, however, requires continued fundamental advances in the science and engineering of materials and in fabrication technologies to enable further improved performance.

References

[1] M. Anderman, Briefing to the U.S. Senate Committee on Energy and Natural Resources, Jan. 26, 2007.
[2] 2006 Annual Progress Report: Energy Storage Research and Development, Energy Efficiency & Renewable Energy, the US Department of Energy.
[3] 2007 Annual Progress Report: Energy Storage Research and Development, Energy Efficiency & Renewable Energy, the US Department of Energy.
[4] Summary Report on "Discussion Meeting on Plug-In Hybrid Electric Vehicles," The US Department of Energy, May 2006.
[5] Basic Research Needs for Electrical Energy Storage, Report for Basic Energy Science Workshop on Electrical Energy Storage, Office of Science, The US Department of Energy, 2007.
[6] J.M. Tarascon, M. Armand, Nature 414 (2001) 359.
[7] J. Maier, Nat. Mater. 4 (2005) 805.
[8] A.S. Arico, P. Bruce, B. Scrosati, J.-M. Tarascon, W. van Schalkwijk, Nat. Mater. 4 (2005) 366.
[9] J. Liu, G. Cao, Z. Yang, D. Wang, D. Dubois, X. Zhou, G.L. Graff, L.R. Pederson, J.-G. Zhang, Chem. Sus Chem. 1 (2008) 676–697.
[10] K.K. Colbow, J.R. Dahn, R.R. Haering, J. Power Sources 26 (1989) 397.

[11] E. Ferg, R.J. Gummov, A. de Kock, M.M. Thackeray, J. Electrochem. Soc. 141 (1994) L147.
[12] T. Ohzuku, A. Ueda, N. Yamamoto, J. Electrochem. Soc. 142 (1995) 1431.
[13] A. Deschanvers, B. Raveau, Z. Sekkal, Mater. Res. Bull. 6 (1971) 699.
[14] S. Takai, M. Kamata, S. Fujine, K. Yoneda, K. Kanda, T. Esaka, Solid State Ion. 123 (1999) 165.
[15] K. Zaghib, M. Simoneau, M. Armand, M. Gauthier, J. Power Sources 300 (1999) 81–82.
[16] D. Peramunage, K.M. Abraham, J. Electrochem. Soc. 145 (1998) 2609.
[17] S. Scharner, W. Weppner, P.S. Beurmann, J. Electrochem. Soc. 146 (1999) 857.
[18] J. Kim, J. Cho, Electrochem. Solid State Lett. 10 (2007) A81–A84.
[19] L. Kavan, M. Grätzel, Electrochem. Solid-State Lett. 5 (2002) A39.
[20] F. Dachille, P.Y. Simons, R. Roy, Am. Mineral. 53 (1968) 1929–1939.
[21] J.E. Post, C.W. Burnham, Am. Mineral. 71 (1986) 142–150.
[22] S. Sodergren, H. Siegbahn, H. Rensmo, H. Lindstom, A. Hagfeldt, S.E. Lindquist, J. Phys. Chem., B 101 (1997) 3087.
[23] A. Henningsson, H. Rensmo, A. Sandell, H. Siegbahn, S. Sodergren, H. Lindstrom, A. Hagfeldt, J. Chem. Phys. 118 (2003) 5607.
[24] C.L. Olson, J. Nelson, M.S. Islam, J. Phys. Chem., B 110 (2006) 9995–10001.
[25] A. Stashans, S. Lunell, R. Begstrom, A. Hagfedt, S.E. Lindquist, Phys. Rev. B 53 (1996) 159–170.
[26] W.C. Mackrodt, J. Solid State Chem. 142 (1999) 428–439.
[27] M.V. Koudriachova, N.M. Harrison, S.W. de Leeuw, Phys. Rev. B 65 (2002) 235423.
[28] M.V. Koudriachova, S.W. de Leeuw, N.M. Harrison, Phys. Rev. B 69 (2004) 054106.
[29] Milman, in: Gonis, et al. (Eds.), Proceedings, 1st International Alloy Conference, Athens, Plenum Press, New York, 1997, p. 19.
[30] A. Navrotsky, O.J. Kleppa, J. Am. Ceram. Soc. 50 (1967) 626.
[31] F. Tielens, M. Calatayud, A. Beltran, C. Minot, J. Andres, J. Electroanal. Chem. 581 (2005) 216–223.
[32] N.M. Gligor, S.W. de Leeuw, Solid State Ion. 177 (2006) 2741–2746.
[33] S. Lunell, A. Stashans, L. Ojamae, H. Lindstrom, A. Hagfeldt, J. Am. Chem. Soc. 119 (1997) 7374–7380.
[34] J.F. Banfield, D.R. Veblen, Am. Mineral. 77 (1992) 545.
[35] D.T. Cromer, K. Herrington, J. Am. Chem. Soc. 77 (1955) 4708.
[36] W.H. Baur, Acta Crystall. 14 (1961) 214.
[37] R. Marchand, L. Brohan, M. Tournoux, Mater. Res. Bull. 15 (1980) 1129.
[38] P.Y. Simons, F. Dachille, Acta Crystall. 23 (1967) 334.
[39] M. Latroche, L. Brohan, R. Marchand, M. Toumoux, J. Solid State Chem. 81 (1989) 78.
[40] H. Sato, S. Endo, M. Sugiyama, T. Kikegawa, O. Shimomura, K. Kusaba, Science 251 (1991) 786.
[41] J. Akimoto, Y. Gotoh, Y. Oosawa, N. Nonose, T. Kumagai, K. Aoki, J. Solid State Chem. 113 (1994) 27.
[42] L. Kavan, M. Graltzel, S.E. Gilbert, C. Klemenz, H.J. Scheel, J. Am. Chem. Soc. 118 (1996) 6716.
[43] T. Ohzuku, Z. Takehara, S. Yoshizawa, Electrochim. Acta 24 (1979) 219.
[44] L. Kavan, D. Fattakhova, P. Krtil, J. Electrochem. Soc. 146 (1999) 1375.
[45] B. Zachau-Christiansen, K. West, T. Jacobsen, S. Atlung, Solid State Ion. 28 (30) (1988) 1176–1182.
[46] W.J. Macklin, R.J. Neat, Solid State Ion. 53 (56) (1992) 694–700.
[47] M.V. Koudriachova, N.M. Harrison, S.W. de Leeuw, Phys. Rev. Lett. 86 (2001) 1275.
[48] M.V. Koudriachova, N.M. Harrison, S.W. de Leeuw, Solid State Ion. 35 (2003) 157.
[49] O.W. Johnson, Phys. Rev. 136 (1964) A284–A290.
[50] F. Gligor, S.W. de Leeuw, Solid State Ion. 177 (2006) 2741–2746.
[51] M.V. Koudriachova, N.M. Harrison, S.W. de Leeuw, Phys. Rev. Lett. 86 (2001) 1275–1278.
[52] A. Stashans, S. Lunell, R. Bergstroem, Phys. Rev. B 53 (1996) 159.
[53] Y.-S. Hu, Kienle Lorenz, Y.-G. Guo, J. Maier, Adv. Mater. 18 (2006) 1421–1426.
[54] E. Baudrin, S. Cassaignon, M. Koesch, J.-P. Jolivet, L. Dupont, J.M. Tarascon, Electrochem. Commun. 9 (2007) 337–342.
[55] C. Delmas, H. Cognac-Auradou, J.-M. Cocciantelly, M. Menetrier, J.P. Doumerc, Solid State Ion. 69 (1994) 257–264.
[56] M. Anji Reddy, M. Satya Kishore, V. Pralong, V. Caignaert, U.V. Varadaraju, B. Raveau, Electrochem. Commun. 8 (2006) 1299–2103.
[57] C. Jiang, I. Honma, T. Kudo, H. Shou, Electrochem. Solid State Lett. 10 (2007) A127.
[58] D. Wang, D. Choi, Z. Yang, V.V. Viswanathan, Z. Nie, C. Wang, Y. Song, J. Zhang, J. Liu, Chem. Mater. 20 (2008) 3435–3442.
[59] C.J. Howard, T.M. Sabine, F. Dickson, Acta Crystallogr., Sec. B, Struct. Sci. 47 (1991) 462.
[60] M. Wagemaker, A.A. van Well, G.J. Kearley, F.M. Mulder, Solid State Ion. 175 (2004) 191–193.
[61] R.J. Cava, D.W. Murphy, S. Zahurak, A. Santoro, R.S. Roth, J. Solid State Chem. 53 (1984) 64.
[62] G. Sudant, E. Baudrin, D. Larcher, J.-M. Tarascon, J. Mater. Chem. 15 (2005) 1263–1269.
[63] J. Li, Z. Tang, Z. Zhang, Electrochem. Solid-State Lett. 8 (2005) A316.
[64] H. Lindström, S. Södergren, A. Solbrand, H. Rensmo, J. Hjelm, A. Hagfeldt, S.-E. Lindquist, J. Phys. Chem. B 101 (1997) 7717–7722.
[65] R. van de Krol, A. Goossens, E.A. Meulenkamp, J. Electrochem. Soc. 146 (1999) 3150–3154.
[66] D.W. Murphy, R.J. Cava, S.M. Zahurak, A. Santoro, Solid State Ion. 9–10 (1983) 413–418.
[67] M. Wagemaker, A.P.M. Kentgens, F.M. Mulder, Nature 418 (2002) 397–399.
[68] M. Wagemaker, G.J. Kearley, A.A. van Well, H. Mutka, F.M. Mulder, J. Am. Chem. Soc. 125 (2003) 840–848.
[69] M. Wagemaker, R. van de Krol, A.P.M. Kentgens, A.A. van Well, F.M. Mulder, J. Am. Chem. Soc. 123 (2001) 11454–11461.
[70] M.V. Koudriachova, N.M. Harrison, S.W. de Leeuw, Solid State Ion. 175 (2004) 829–834.
[71] M. Wagemaker, W.J.H. Borghols, F.M. Mulder, J. Am. Chem. Soc. 129 (2007) 4323–4327.
[72] L. Kavan, M. Kalbac, M. Zukalova, I. Exnar, V. Lorenzen, R. Nesper, M. Graetzel, Chem. Mater. 16 (2004) 477–485.
[73] M. Zukalova, M. Kalbac, L. Kavan, I. Exnar, M. Graetzel, Chem. Mater. 17 (2005) 1248–1255.
[74] X.P. Gao, Y. Lan, H.Y. Zhu, J.W. Liu, Y.P. Ge, F. Wu, D.Y. Song, Electrochem. Solid-State Lett. 8 (2005) A26.
[75] J. Xu, C. Jia, B. Cao, W.F. Zhang, Electrochem. Acta 52 (2007) 8044–8047.
[76] J. Kim, J. Cho, J. Electrochem. Soc. 154 (2007) A542–A546.
[77] S.-J. Bao, Q.-L. Bao, C.-M. Li, Z.-L. Dong, Electrochem. Commun. 9 (2007) 1233–1238.
[78] T.P. Feist, P.K. Davies, J. Solid State Chem. 101 (1992) 275.
[79] A.R. Armstrong, G. Armstrong, J. Canales, R. Garcia, P.G. Bruce, Adv. Mater. 17 (2005) 862.
[80] A.R. Armstrong, G. Armstrong, J. Canales, P.G. Bruce, J. Power Sources 146 (2005) 501.
[81] A.R. Armstrong, G. Armstrong, J. Canales, P.G. Bruce, Angew. Chem. Int. Ed. 43 (2004) 2286.
[82] G. Armstrong, A.R. Armstrong, P.G. Bruce, P. Reale, B. Scrosati, Adv. Mater. 18 (2006) 2597.
[83] A.S. Arico, P. Bruce, B. Scrosati, J.-M. Tarascon, W.V. Schalkwijk, Nat. Mater. 4 (2005) 366–377.
[84] M. Anji Reddy, V. Pralong, U.V. Varadaeaju, B. Raveau, Electrochem. Solid-State Lett. 11 (8) (2008) A132–A134.
[85] M. Anji Reddy, M. Satya Kishore, V. Pralong, U.V. Varadaraju, B. Raveau, Electrochem. Solid-State Lett. 10 (2) (2007) A29–A31.
[86] Du-Hee Lee, Jae-Gwan Park, Kyoung Jin Choi, Heon-Jin Choi, Dong-Wan Kim, Eur. J. Inorg. Chem. (2008) 878–882.
[87] Y.-G. Guo, Yong-Sheng Hu, W. Sigle, J. Maier, Adv. Mater. 19 (2007) 2087–2091.
[88] D. Wang, D. Choi, J. Li, Z. Yang, Z. Nie, R. Kou, C. Wang, L.V. Saraf, J. Zhang, I.A. Aksay, J. Liu, ACS Nano, in press.
[89] H. Zhou, D. Li, M. Hibino, I. Honma, Angew. Chem. Int. Ed. 44 (2005) 797–802.